Doping Effects in Single-Layered $La_{0.5}Sr_{1.5}MnO_4$ Manganite

Lorenzo Malavasi,*,† Maria Cristina Mozzati,‡ Clemens Ritter,§ Vladimir Pomjakushin,|| Cristina Tealdi,† Carlo Bruno Azzoni,‡ and Giorgio Flor†

Dipartimento di Chimica Fisica "M. Rolla", INSTM, Università di Pavia, Via le Taramelli 16, I-27100, Pavia, Italy, Dipartimento di Fisica "A. Volta" and CNISM, Università di Pavia, Via Bassi 6, I-27100, Pavia, Italy, Institute Laue-Langevin, Boite Postale 156, F-38042, Grenoble, France, and Laboratory for Neutron Scattering, ETHZ and PSI, CH-5232 Villigen PSI, Switzerland

Received: June 1, 2006; In Final Form: July 13, 2006

In this paper we report the results of the synthesis and structural, transport, and magnetic characterization of pure $La_{0.5}Sr_{1.5}MnO_4$ and B-site lightly doped samples, i.e. $La_{0.5}Sr_{1.5}Mn_{0.95}B_{0.05}O_4$, where B = Ru, Co, and Ni. The choice was made in order to probe the charge ordering/orbital ordering ground state of the monolayered $La_{0.5}Sr_{1.5}MnO_4$ manganite as a consequence of the cation doping. It is shown that even a light doping is successful in suppressing the charge and orbital order found in pure $La_{0.5}Sr_{1.5}MnO_4$. No long-range magnetic order has been detected in any of the doped samples but the setup of a spin-glass state with a common freezing temperature (∼22 K). Structural parameters show an anisotropy in the lattice constant variation, with the tetragonal distortion increasing as the cell volume reduces, which may suggest a variation in the orbital character of the e_g electrons along with the overall cation size.

1. Introduction

In recent times there has been a revitalization of interest in the manganites as a result of the wide range of physical properties they display. In some of the doped compounds, there is an ordering of the charge carriers in defined orbitals, resulting in orbital ordering (OO) and charge ordering (CO). This is particularly true for the $n = 1$ members of the Ruddlesden−Popper (R−P) series of manganites of general formula $A_{n+1}Mn_nO_{3n+1}$ in which n 2D layers of MnO_6 corner-sharing octahedra are joined along the stacking direction and separated by rock-salt AO layers. Lowering the dimensionality of these systems makes compounds such as the $La_{1+x}Sr_{1-x}MnO_4$ (LSMO) solid solution an interesting model system for the study of the underlying doped MnO_2 planes and for a comparison with results for the double-layer ($n = 2$) and perovskite ($n = \infty$) manganites.

In particular, in the $La_{0.5}Sr_{1.5}MnO_4$ compound, the Mn ions are nominally present in equal amounts in the +3 and +4 oxidation state and do order at around 240 K (CO), where it is believed that charge disproportionation of Mn ions occurs, leading to two inequivalent sites for Mn^{3+} and Mn^{4+} ions.[1−4] At temperatures lower than 110 K an anti-ferromagnetic (AF) order takes place, where the spin of neighboring Mn ions aligns antiferromagnetically within the MnO_2 planes. However, no trace of long-range magnetic order has been found in these compounds, where a spin-glass behavior is instead observed, in accordance with the theoretical prediction of the absence of long-range magnetic order in one- or two-dimensional Heisenberg models.[5]

It is interesting to note that the setup of CO is accompanied by an OO of the e_g orbitals. This OO seems to be the dominant effect in $La_{0.5}Sr_{1.5}MnO_4$: recent resonant soft X-ray diffraction experiments at the Mn-L edges have shown that the OO starts at the CO temperature and progressively increases by reducing the temperature, and, in addition, it strongly increases at the Neél temperature.[3] Moreover, this study[3] revealed that the two major causes of the OO are the Jahn−Teller distortion and the short-range antiferromagnetic spin correlations. It is clear that the definition of the final ground state of $La_{0.5}Sr_{1.5}MnO_4$ is finely tuned by the AF exchange interactions in the presence of a strong anisotropy.

Foreign atoms doping represents an interesting way to investigate the relative stability of the competing magnetic interactions within the orbitally ordered $La_{0.5}Sr_{1.5}MnO_4$ manganite. For this purpose in this paper we are interested in looking at the role of low cation doping (5%, $x = 0.05$) on the B-site of the structure. We carried out the synthesis and structural, transport, and magnetic characterization of $La_{0.5}Sr_{1.5}Mn_{0.95}B_{0.05}O_4$ samples, where B = Ru, Co, and Ni. We stress that among these ions, only Ru-doping was already studied on the $La_{0.5}Sr_{1.5}MnO_4$ compound for $0.1 \leq x \leq 0.5$, where, for doping higher than 10%, a ferromagnetic (F) component coming from the Mn/Ru site has been observed.[6] As a consequence, it seems that, also in order to fill the composition gap for the Ru-doped $La_{0.5}Sr_{1.5}MnO_4$, a lower doping level with respect to the ones already studied in the literature is needed.

All the data collected in this work have been compared to the properties of the pure $La_{0.5}Sr_{1.5}MnO_4$ manganite. Samples characterization was carried out by means of X-ray powder diffraction, neutron diffraction, DC transport measurements, magnetometry, and electron paramagnetic resonance.

2. Experimental Section

$La_{0.5}Sr_{1.5}Mn_{0.95}B_{0.05}O_4$ samples, where B = Mn (pure LSMO), Ru, Co, and Ni were synthesized through a wet-chemistry method defined as "propellant chemistry". In this route that we previously applied to the synthesis of perovskite manganites,[7]

* Corresponding author. Telephone: +39-(0)382-987921. Fax: +39-(0)382-987575. E-mail: lorenzo.malavasi@unipv.it.
† INSTM, Università di Pavia.
‡ Dipartimento di Fisica "A. Volta" and CNISM, Università di Pavia.
§ Institute Laue-Langevin.
|| ETHZ and PSI.

10.1021/jp063384+ CCC: $33.50
Published on Web 08/17/2006

proper amounts of metal nitrates (all Aldrich ≥99.99+%) were used as oxidizers, while a slight excess of urea (Carbonyldiamide, CH_4N_2O, Fluka >99.5%) was used as fuel. The oxidizers and fuel were dissolved in a small quantity of deionized water and heated on a hot-plate to 473 K until the whole solvent was evaporated. The final spongy powder was then calcined in a platinum crucible to 1023 K for 1 h. Finally, the powders were pressed and heated to 1573 K for 70 h.

X-ray powder diffraction (XRPD) patterns were acquired on a "Bruker D8 Advance" diffractometer equipped with a Cu anode in the 2θ range from 10 to 140° with a step size of 0.02°.

Neutron powder diffraction (NPD) data for $La_{0.5}Sr_{1.5}Mn_{0.95}B_{0.05}O_4$ (B = Ru, Co, and Ni) were collected at the D1A instrument at the ILL Facility in Grenoble with a wavelength of 1.39 Å at room temperature (RT) and of 1.91 Å at low temperature (10 K). Neutron patterns for pure $La_{0.5}Sr_{1.5}MnO_4$ manganite were acquired on the HPRT instrument[8] of Swiss spallation source SINQ at PSI with a wavelength of 1.15 Å at RT and of 1.89 Å at low temperature (15 K).

Neutron data were refined by means of FULL-PROFILE software.[9] The parameters refined were zero shift, scale factor, background, lattice constants, atomic positions, fractional occupancies, and isotropic thermal factors.

Static magnetization was measured at 100 Oe from 350 K down to 2 K with a SQUID magnetometer (Quantum Design). *M* vs *H* curves up to 70 000 Oe have been also collected (at 5 K).

Electron paramagnetic resonance (EPR) measurements were performed at ~9.5 GHz with a Bruker spectrometer, with a continuous nitrogen flow used to study the temperature dependence in the range 140−470 K.

Resistivity measurements were carried out with the DC-four electrodes method.

3. Results

3.1. Structural Characterization. Room-temperature XRPD characterization of pure $La_{0.5}Sr_{1.5}MnO_4$ (LSMO) and $La_{0.5}Sr_{1.5}Mn_{0.95}Ru_{0.05}O_4$ (LSMRO), $La_{0.5}Sr_{1.5}Mn_{0.95}Co_{0.05}O_4$ (LSMCO), and $La_{0.5}Sr_{1.5}Mn_{0.95}Ni_{0.05}O_4$ (LSMNO) samples revealed the single-phase nature of all the compounds. They all crystallize in the tetragonal *I*4/*mmm* space group without any detectable deviations from this symmetry. Figure 1 shows, as a selected example, the Rietveld refined XRPD pattern of the pure LSMO compound together with a sketch of the crystal structure (R_{wp} for the Rietveld refinement is 10.4).

Room-temperature NPD was used to refine the structural details due to the higher reliability of NPD, with respect to XRPD, in determining the atomic positions and thermal parameters, particularly when considering light atoms such as oxygen. Figure 2 reports, as a selected example, the room-temperature refined neutron pattern for pure LSMO (R_{wp} = 2.7). Structural parameters derived from the patterns refinement are listed in Table 1.

Figure 3 shows the *a* and *c* lattice constants trend against the dopant ions, according to a descending order of the ionic radii considering an equal formal valence and coordination for all of them, while the cell volume and *c*/*a* parameter behavior as a function of dopant ions are plotted in Figure 4. Here and in the following figures "Mn" represents the pure $La_{0.5}Sr_{1.5}MnO_4$ sample.

As can be appreciated from Figure 3, an anisotropy is present in the behavior of the lattice parameters along with the cation replacement: the *a* axis progressively shrinks, passing from the pure sample to the Co-doped one, while the *c* axis first contracts

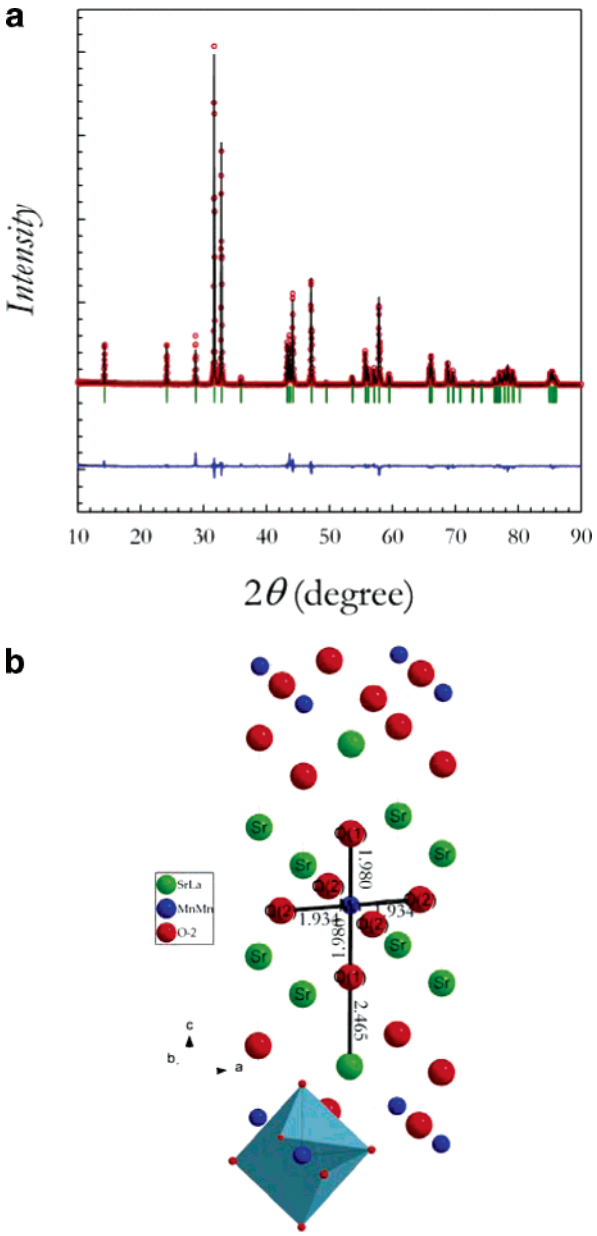

Figure 1. (a) Refined X-ray diffraction pattern of $La_{0.5}Sr_{1.5}MnO_4$. Red crosses represent the experimental pattern, and the black line is the calculated one, while the blue line is the difference between them. Bragg peaks appear as vertical green lines. (b) Sketch of the *I*4/*mmm* crystal structure of the single-layered manganite.

going from $La_{0.5}Sr_{1.5}MnO_4$ to $La_{0.5}Sr_{1.5}Mn_{0.95}Ru_{0.05}O_4$ and then progressively expands along with the cation replacement. Overall, the cell volume (see Figure 4) reduces, while the tetragonal distortion (*c*/*a*) increases, passing from $La_{0.5}Sr_{1.5}MnO_4$ to $La_{0.5}Sr_{1.5}Mn_{0.95}Co_{0.05}O_4$. It must be noted, however, that pure and Ru-doped samples have similar values of both the cell volume and the *c*/*a* parameter and that a significant change in the two constants occur when Ni and Co are introduced in the lattice. Ni- and Co-doped samples have close structural parameter values.

Figure 5 displays the trend of Mn−O bond lengths as a function of the dopant ion. Two distinct Mn−O bonds are present in single-layered manganites: a longer out-of-plane bond labeled as Mn−O(1) (axial) and a shorter in-plane bond labeled Mn−O(2) (equatorial) (see also the structure of Figure 1 for reference). Both Mn−O bonds shrink going from $La_{0.5}Sr_{1.5}MnO_4$

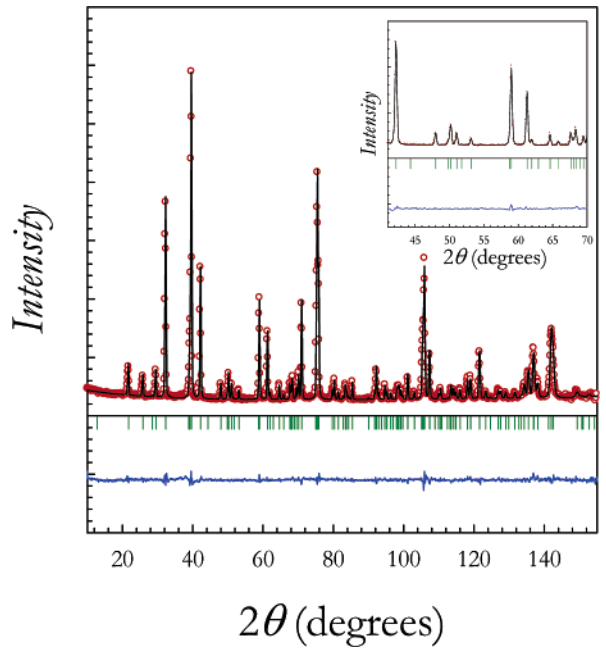

Figure 2. Refined neutron diffraction pattern of $La_{0.5}Sr_{1.5}MnO_4$. Red crosses represent the experimental pattern, and the black line is the calculated one, while the blue line is the difference between them. Bragg peaks appear as vertical green lines. Inset: detail of a pattern region.

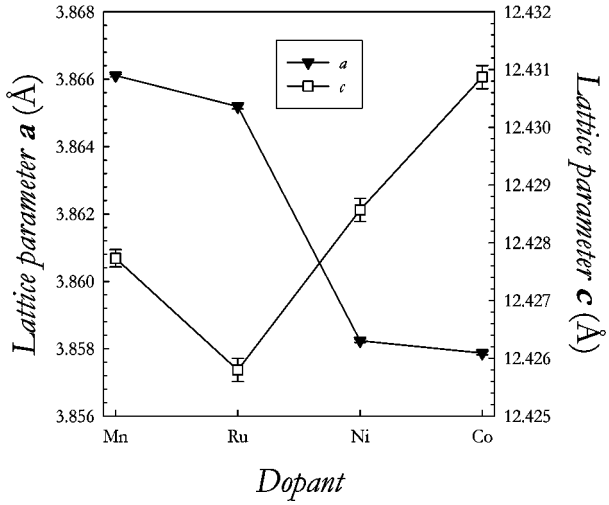

Figure 3. *a*, *c* lattice constants for the different cation-doped LSMO samples.

TABLE 1: Structural Parameters Derived from the Neutron Diffraction for the $La_{0.5}Sr_{1.5}Mn_{0.95}B_{0.05}O_4$, Where B = Ru, Mn (Pure Sample), Ni, and Co

	Ru	Mn	Ni	Co
a (Å)	3.86519(7)	3.86610(5)	3.85823(5)	3.85786(5)
c (Å)	12.4257(2)	12.4277(1)	12.4285(2)	12.4308(2)
V (Å^3)	185.638(5)	185.755(4)	185.012(4)	185.011(4)
c/*a*	3.2147(3)	3.2145(2)	3.2213(2)	3.2222(2)

to $La_{0.5}Sr_{1.5}Mn_{0.95}Co_{0.05}O_4$. However, a sort of "jump" in the bond shortening is apparent for the Mn−O(2) length passing from the Ru- to the Ni-doped sample; on the opposite, for the Mn−O(1) length, the reduction looks smoother. Overall, the average Mn−O bond length slightly contracts in the same direction, as shown in the inset of Figure 5.

The variation of the structural parameters is discussed as a function of the nature of cations on the B-site. This may be useful to get some information about the average oxidation state

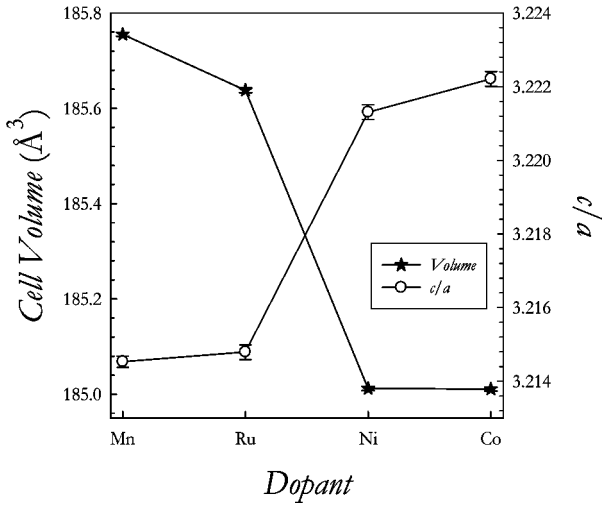

Figure 4. Cell volume and *c*/*a* parameter for the different cation-doped LSMO samples.

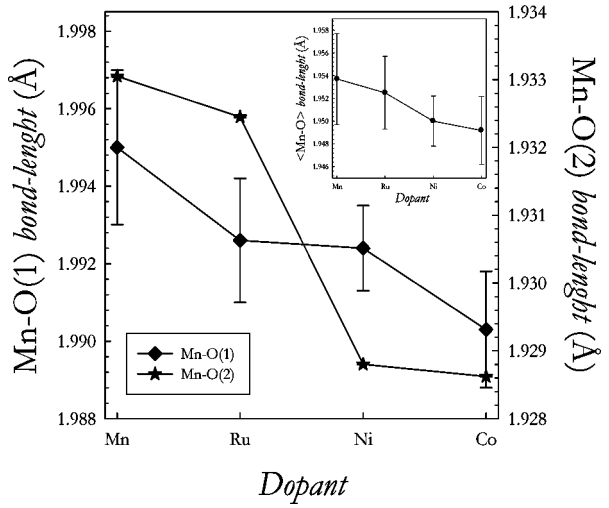

Figure 5. Axial and equatorial Mn−O bonds for the different cation-doped LSMO samples. Inset: average Mn−O bond length for the same samples.

of dopant ions in the structure by considering the ionic radii of all the ions for the same coordination.[10]

Doping pure $La_{0.5}Sr_{1.5}MnO_4$ with 5% Ru, Co, or Ni induces a cell contraction. The reduction of cell volume by Ru doping rules out the presence of Ru^{3+}, which has an average ionic radius for the octahedral coordination of 0.68 Å. However, the presence of only Ru^{4+} ions should in any case lead to a *V* increase. Consequently, it appears that the most probable valence state for Ru in $La_{0.5}Sr_{1.5}MnO_4$ is a mixed state between +4 and +5, as also suggested by previous authors.[11] Both Ni- and Co-doped samples have smaller lattice volumes than pure $La_{0.5}Sr_{1.5}MnO_4$. On the basis of the ionic radii for the various possible oxidation states and electronic configurations of Ni and Co in an octahedral environment, it can be concluded that nickel is present only as Ni^{3+} with a low-spin (LS) configuration ($t_{2g}^6e_g^1$), while we cannot be conclusive on the Co state, since LS Co^{3+} and Co^{4+} ions have very similar ionic radii (0.545 and 0.530 Å, respectively). Most probably, also the Co ions are present in a mixed valence state. However, the divalent state for cobalt is hardly possible based on the lattice volume. This result is in contrast to what is found in charge-ordered perovskite manganites, i.e. the analogous $n = \infty$ member of the R−P series of the LSMO single-layered manganite, where a stable Co^{2+} valence state was observed.[12] We also stress that aliovalent ion

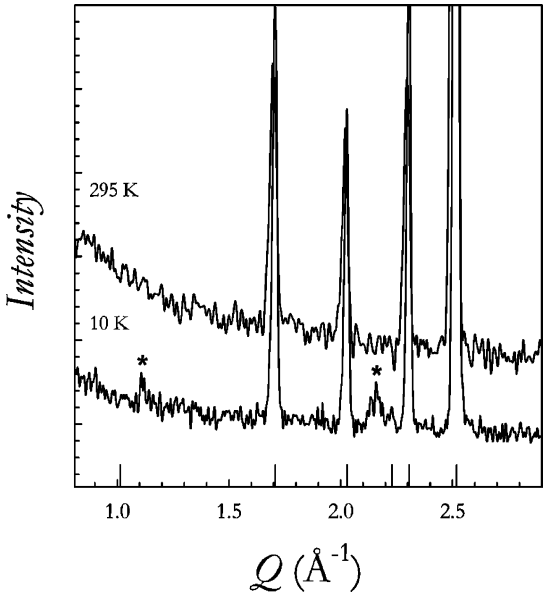

Figure 6. NPD pattern at 295 and 10 K for the $La_{0.5}Sr_{1.5}Mn_{0.95}Ru_{0.05}O_4$. Asterisks mark the extra peaks found in the low-temperature pattern.

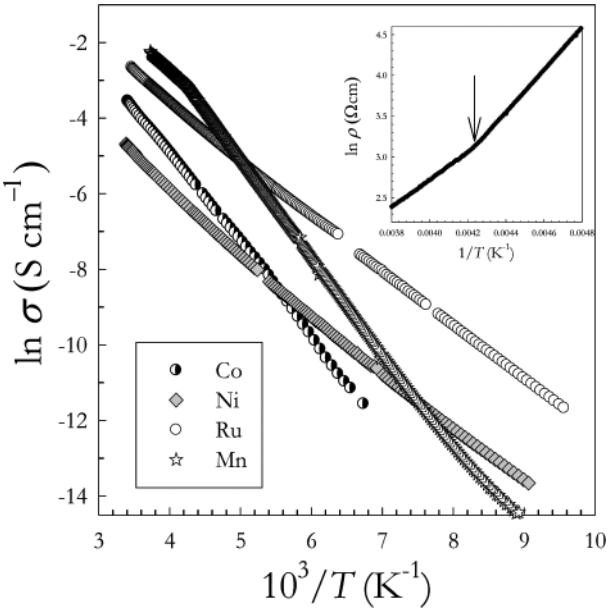

Figure 7. Logarithm of conductivity (σ) vs $1/T$ for the $La_{0.5}Sr_{1.5}Mn_{0.95}B_{0.05}O_4$ samples, where B = Ru, Mn (pure sample), Ni, and Co. In the inset is reported the logarithm of ρ vs $1/T$ for $La_{0.5}Sr_{1.5}MnO_4$ with the arrow highlighting the slope change around the CO temperature.

doping may induce a slight variation in the oxidation state of Mn ions as a consequence of charge compensation mechanism between dopant ions and manganese. This last aspect will be studied in detail in planned X-ray absorption spectroscopy experiments.

The trend shown in Figure 3 interestingly suggests that the unit cell does not expand in an isotropic way as the size of the ions increases. This in turn may witness the presence of an electronic factor playing a role in the definition of the structural features of the samples.

Overall, the cell reduction follows the ionic radii difference between the ions, all the dopants being smaller than the "hypothetical" $Mn^{3.5+}$ ion. However, the significant increase of the tetragonal distortion for Ni- and Co-doped samples follows the *a*-parameter trend (Figure 3) that in turn can be linked to the peculiar behavior of the in-plane Mn−O(2) bond length (Figure 5). The Mn−O(2) bond length is strongly influenced by the Ni and Co cation replacement with respect to the out-of-plane Mn−O(1) bond, which, on the other hand, seems to smoothly follow the simple "size effect", except for the plateau between Ru and Ni. The fact that the out-of-plane bond does not lengthen, passing from the Ru- to the Ni-doped sample, where the in-plane bond anomalously decreases, suggests that in these two samples a stabilization of the out-of-plane static J−T distortion and of the $d_{3z^2-r^2}-e_g$ orbitals occurs.

Neutron data were also collected at 10 K in order to (mainly) look for possible magnetic superstructure peaks. Careful inspection of all the low-*T* patterns did not reveal the presence of any clear peak coming from the magnetic long-range order or any significant intensity enhancement of nuclear peaks.

For pure $La_{0.5}Sr_{1.5}MnO_4$ the low-*T* pattern revealed the presence of two broad and low-intensity peaks that can be indexed according to the proposed magnetic unit cell with magnetic scattering vectors at (1/2;1/2;1/2) and (1/2;0;1/2).[2] In the case of the Ru-doped sample it was possible to observe the presence, with respect to the room-temperature pattern, of very broad and low-intensity extra peaks, as well.

Figure 6 reports a detail of the neutron powder patterns at 295 and 10 K for the $La_{0.5}Sr_{1.5}Mn_{0.95}Ru_{0.05}O_4$ sample. Peaks marked with the asterisk are only present in the low-temperature pattern. The two peaks cannot be directly connected to the magnetic cell of the pure compound. In addition, contrary to heavily Ru-doped samples,[10] $La_{0.5}Sr_{1.5}Mn_{0.95}Ru_{0.05}O_4$ does not present a clear ferromagnetic order as witnessed by the good refinement of the intensity of those peaks, like the (101), by considering only the nuclear contribution. Overall, the additional broad peaks in the pattern collected at 10 K are indicative of short-range magnetic interactions as encountered in spin-glass materials and originating from the competition between F and AF order.

TABLE 2: Activation Energies and ρ-Values at 260 K for the Samples Considered

sample	E_a (meV)	ρ_{260K} (Ω cm)
$La_{0.5}Sr_{1.5}MnO_4$	144−212	11.7
$La_{0.5}Sr_{1.5}Mn_{0.95}Ru_{0.05}O_4$	135	27.3
$La_{0.5}Sr_{1.5}Mn_{0.95}Co_{0.05}O_4$	200	92.5
$La_{0.5}Sr_{1.5}Mn_{0.95}Ni_{0.05}O_4$	154	265.1

3.2. Electrical Transport Properties. On all the samples considered here we performed low-temperature four-probe DC electrical conductivity measurements. Figure 7 reports the ln σ vs $1/T$ plots obtained. Temperature ranges explored are in some cases reduced due to the very low σ-values of the samples, particularly at low *T*.

Activation energies, E_a, calculated by considering a purely activated transport according to

$$\sigma = \sigma_\infty(E_a/KT) \qquad (1)$$

are reported in Table 2 together with the resistivity values at 260 K for all the samples.

Pure $La_{0.5}Sr_{1.5}MnO_4$ has a high variation of the resistivity values in the investigated *T* range and presents (see inset of Figure 7) a clear slope change around 240 K, i.e., around the CO/OO temperature (corresponding to the cusp in the χ_{mol} vs *T* curve). As consequence, for this sample two different values of the activation energy are estimated and listed in Table 2: the lower value refers to the data from room temperature to the slope change at around 240 K, while the higher value pertains to the data after this temperature. Note that no clear sign of the

AF order is found in the σ vs T curve, in agreement with the results found by other authors.[13,14]

For all the cation-doped samples the slope change observed at 240 K for LSMO is absent. Indeed, in the doped samples, the CO/OO, as well as the AF order, is not present anymore (see next paragraph). In the range above the temperature of the CO/OO transition of the pure sample, a general increase of the electrical resistivity occurs along with the cation doping (see in Table 2 the ρ values for all the samples at 260 K). Comparable E_a values are obtained for all the samples but for the Co-doped one, which shows the highest E_a value. These results suggest that the cation doping (Co, in particular) generally hinders the charge carrier transport in the temperature region before the CO of the pure sample. This may be related to a chemical disorder effect induced by the doping with ions of different size. For $T < 240$ K all the doped samples present a reduction of the activation energies with respect to the pure one (see Table 2), thus suggesting the cation doping is effective in promoting the charge carrier transport, at least in this temperature range: Co ions, and even more Ni and Ru ions, give origin to an enhancement of the electron hopping by reducing the E_a with respect to the pure sample in its CO regime. It is fair to think that the effect of the dopants in this T region is mainly related to the removal of the CO state.

On the other hand the hopping of charge carriers is influenced by structural parameters. It looks that a direct correlation between the hopping energy and the overall c/a tetragonal distortion is present: as the tetragonal distortion increases passing from 3.2147(3) for the Ru-doped sample to 3.2222(2) for the Co-doped samples, the E_a rises from 135 to 200 meV.

Besides, it is clear that by lowering the temperature the conductivity of the pure sample reduces much more than the conductivity of the doped samples, probably due to the progressive evolution of the AF order which, generally, strongly hinders the hopping mechanism. Among the doped samples the highest σ-values at low T correspond to the $La_{0.5}Sr_{1.5}Mn_{0.95}Ru_{0.05}O_4$ material. This is probably connected to the possibility of magnetic exchange between dopant ion and Mn ions with the creation of short-range magnetic interactions that may constitute preferential conduction pathways. In addition, for the Ru-doped sample the more expanded nature of the 4d orbitals could be a further origin of the "better" conductivity induced by this dopant with respect to Ni and Co.

3.3. Magnetic Properties. Figure 8 shows the zero-field-cooling (ZFC) and field-cooling (FC) molar susceptibility at 100 Oe for the samples studied in this work. In the inset are put in prominence the ZFC and FC curves for the pure $La_{0.5}Sr_{1.5}MnO_4$.

Pure LSMO presents two transitions, which are clear in the FC curve (marked with arrows in the inset of Figure 8): a first cusp at around 240 K (CO/OO transition) and a minimum around 110−120 K which marks the AF transition. However, we note that this AF phase is not a long-range ordered phase but, overall, the sample behaves as a spin-glass. This is consistent with the theoretical prediction of the absence of long-range magnetic order in 2D Heisenberg systems. In particular the AF phase found in this system extends as long range only in the $a-b$ plane, while it has a finite correlation length perpendicular to the MnO_2 planes.[3]

Doped samples do not present any sign of the magnetic transitions found in the pure sample. In detail, the Ni-doped sample behaves as a pure paramagnet for temperatures up to ~25 K, while for lower temperatures the FC and ZFC curves deviate one from each other. This implies the evolution of a magnetic order which, on the basis of the neutron data, is not a long-range order. An analogous trend is found for both the Ru- and Co-doped LSMO. However, for these two samples the setup of magnetic interactions starts at higher temperatures with respect to the Ni-doped LSMO, and in particular a separation between the FC and ZFC curves for the $La_{0.5}Sr_{1.5}Mn_{0.95}Co_{0.05}O_4$ is already present at room temperature. We note that the shape of the susceptibility curves for all the doped samples resembles that of a spin-glass, particularly for the presence of a distinct maximum in the ZFC. Interestingly, the peak in the ZFC curves, which can be thought of as the freezing transition to the low-temperature phase with random alignment of the spins, falls at nearly the same temperature, ~22 K, for all the samples, thus suggesting the presence of the same type of magnetic interaction for all of them even though with different strength from sample to sample. The origin of the magnetic frustration in these samples is probably due to the presence of competing F and AF interactions and from the disorder induced by the cation doping.

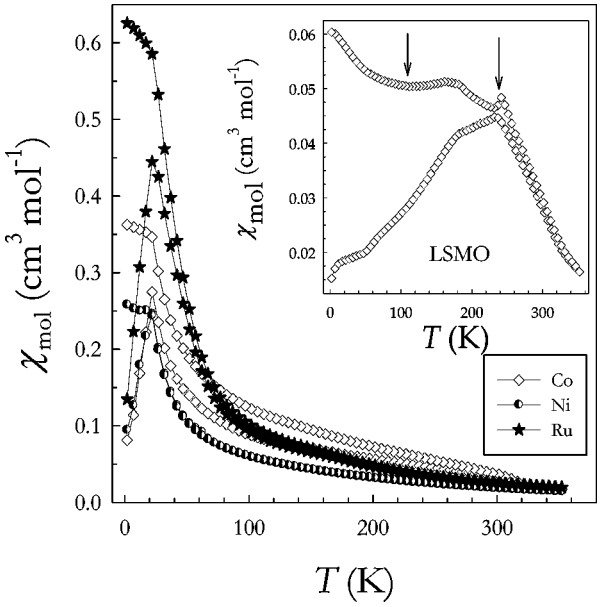

Figure 8. Molar magnetic susceptibility vs T for the $La_{0.5}Sr_{1.5}Mn_{0.95}B_{0.05}O_4$ samples, where B = Ru, Mn (pure sample, in the inset), Ni, and Co. Both FC and ZFC curves are shown.

Finally, Figure 9 presents the field dependence of the magnetization of all the samples at 5 K. Only for pure LSMO there is an almost linear dependence of M with the field, while for all the other samples a marked curvature occurs, even if the magnetization never saturates, according to the short-range nature of the magnetic interactions. From the linear part of the M vs H curves the paramagnetic contribution can be estimated. For the doped samples, values of 1 order of magnitude less that the expected ones in the case of pure paramagnetism are obtained. However, these experimental values are more than two times higher than that obtained for the pure sample. This suggests that, for the concentrations here considered, the dopant ions, whatever is their nature, hinder the magnetic interactions responsible of the short-range AF order pertinent for the pure sample. This is also in agreement with the neutron diffraction measurements performed.

The comprehension of the magnetic behavior can be deepened by looking at the temperature dependence of the EPR signals, as previously done on Ca- and Na-doped lanthanum manganite perovskite.[15,16] The EPR spectrum of the $n = \infty$ manganites (i.e., perovskites), which are characterized by a para- to

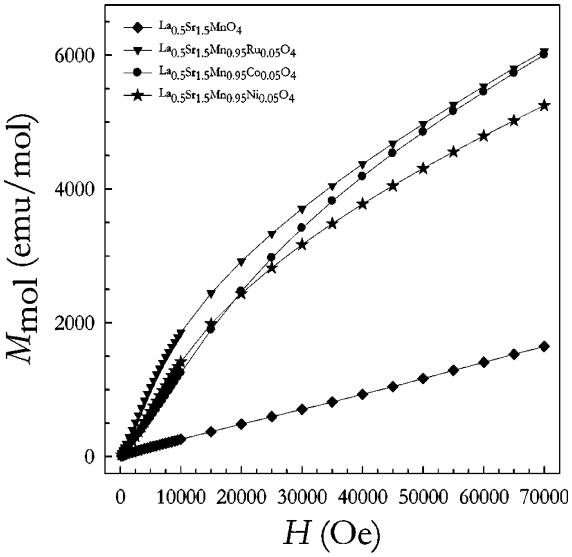

Figure 9. Magnetization vs H at 5 K for the $La_{0.5}Sr_{1.5}Mn_{0.95}B_{0.05}O_4$ samples, where B = Ru, Mn, Ni, and Co.

ferromagnetic (P−F) transition, arises from Mn(IV) single ions or from Mn(III)−Mn(IV) Zener pairs.[17] The spectrum evolves from a single signal with g-value ≅ 2 at high temperatures, corresponding to the paramagnetic phase, to a single signal with g-value > 2 at low temperatures, which is direct evidence of the presence of internal magnetic fields resulting from homogeneous ferromagnetic interactions in the whole sample. In the intermediate temperature range (corresponding to the onset and completion of the broad magnetic transition) two or more components with different g-values are detectable, indicating the presence of local inhomogeneous internal magnetic fields in different sample regions.

Most of the features described above for the perovskite manganites characterize the spectra of the samples considered in this work. Figure 10 reports a detailed temperature dependence of the EPR spectrum of the pure LSMO sample. At the highest investigated temperatures a broad signal with g-value ≅ 2 (paramagnetic phase) is observed together with a very narrow signal ascribable to a negligible impurity paramagnetic phase (it corresponds at about 0.02% of the total EPR centers, as obtained by a comparison of the signal areas). By decreasing the temperature a second component, centered at $g > 2$, appears at about 350 K, as put in prominence by the results of the spectrum simulation obtained from numerical analysis. This is in agreement with the susceptibility curve which never shows a purely paramagnetic behavior even at the highest investigated temperatures (352 K). By further lowering the temperature, additional components appear in the simulated spectrum and move toward lower resonant fields, thus evidencing the progressive formation of magnetic domains. An example of the signal simulation is reported in Figure 11, where the experimental curve detected at 320 K is compared to the computed one. In the same figure all the components of the spectrum are separately shown. Only around the temperature of the CO ordering a clear separation of the experimental signal in two main components can be observed. We can thus distinguish between a component related to the magnetic domains, the one with $g > 2$, and the main component, i.e., the broad signal with g-value ≅ 2 that progressively broadens by lowering the temperature while keeping its g-value practically constant, as can be expected when the system evolves toward an AF transition.[18] We point out that this main component practically disappears at the lowest temperature investigated, 140 K, i.e.,

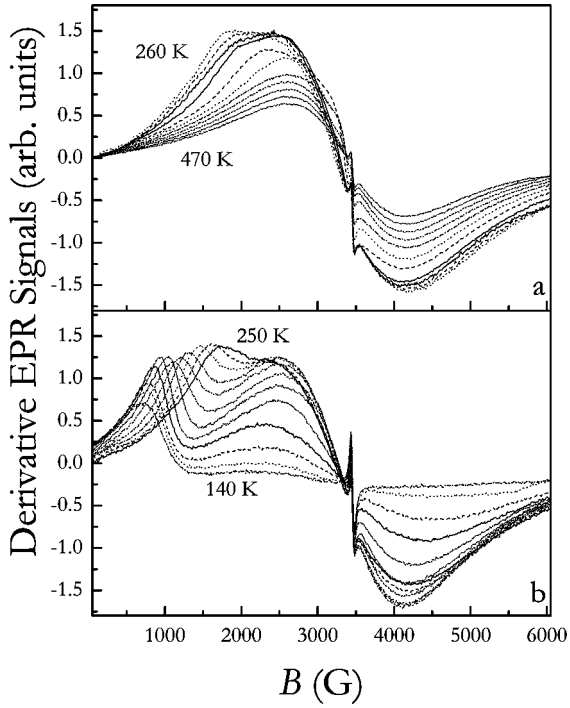

Figure 10. Temperature dependence of the derivative EPR signal of pure LSMO: (a) spectra collected from 470 to 260 K (intermediate temperatures are 445, 420, 395, 370, 345, 320, 295, 280, and 270 K); (b) spectra collected from 250 to 140 K (intermediate temperatures are 240, 230, 220, 210, 200, 190, 180, 170, 160, and 150 K).

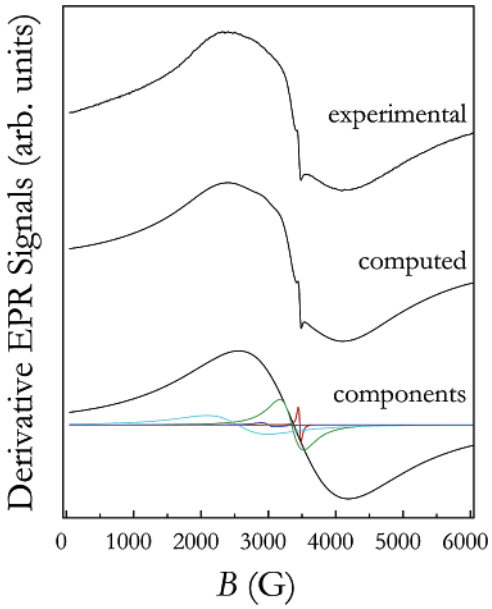

Figure 11. Experimental and computed (from numerical analysis) derivative EPR signal of pure LSMO sample at 320 K. All the components of the computed signal are also shown.

near the AF transition that, in this sample, occurs at 110 K. The behavior of the main component with the temperature is the principal difference between the EPR spectrum of the single-layered LSMO and the $n = \infty$ manganites described above.

The temperature dependence of the EPR spectrum for all the doped samples considered here is in agreement with the magnetic susceptibility curves and confirms the influence of cation doping on the magnetic interactions. Indeed, in the investigated temperature range, no evidence of shift of the resonant field or separation of the signal in two or more components occurred for the Ni-doped sample. For the Co-doped

one an asymmetric signal with g-factor > 2 and which moves toward lower resonant fields by lowering the temperature is already observed at 320 K; this is the temperature of the separation between ZFC and FC susceptibility curves, even though no clear separation of the signal in two or more components is detected. Finally, the Ru-doped sample displays a very broad spectrum that further broadens by lowering the temperature, but always with the same g-value.

Overall, the cation doping on the B-site induces a size-effect ("chemical disorder") and a slight variation of the Mn-valence state. In particular, if we consider as the possible valence states of the dopant ions those indirectly determined from the lattice effects, we may note that the Ni doping can be considered analogous to a Mn oxidation, which, on the basis of the phase diagram published by Larochelle and co-authors,[19] should lead to the evolution of an AF phase with a T_N higher than 100 K. However, it is clear from our data that no long-range AF order is present in the Ni-doped $La_{0.5}Sr_{1.5}MnO_4$, thus putting in prominence the effect of cation disorder on the magnetic proprieties of the doped compound.

For the $La_{0.5}Sr_{1.5}Mn_{0.95}Ru_{0.05}O_4$ sample the Mn oxidation state should be reduced as a consequence of the average Ru valence higher than 3.5. In this case, again on the basis ref 19, we should expect a short-range order and spin-glass state below ~25 K, which is in agreement with our data. Finally for the Co-doping it is not easy to draw any conclusion due to a high uncertainty about the possible valence state of the dopant ions.

4. Conclusion

In this paper we reported the results of an investigation which aimed at studying the role of cation doping on the B-site (Mn) of the single-layered $La_{0.5}Sr_{1.5}MnO_4$ manganite. The main results we obtained can be summarized in the following:

(1) We successfully synthesized single-phase tetragonal $La_{0.5}Sr_{1.5}Mn_{0.95}Ru_{0.05}O_4$, $La_{0.5}Sr_{1.5}Mn_{0.95}Co_{0.05}O_4$, and $La_{0.5}Sr_{1.5}Mn_{0.95}Ni_{0.05}O_4$ samples. The last two have never been prepared and characterized before. In addition, we employed for the preparation of these compounds, for the first time, a wet-chemistry method that was previously used to prepare doped $LaMnO_3$ samples.[7]

(2) Structural parameters show an anisotropy in the lattice constant variation, with the tetragonal distortion increasing as the cell volume reduces; this may suggest a variation in the relative nature of the orbital character of the e_g electrons along with the overall cation size.

(3) CO/OO and AF transitions characterizing the pure LSMO disappear in all the doped samples, thus suggesting that a light doping, as the one realized here, is already able to destroy the orbital ordered ground state of the $La_{0.5}Sr_{1.5}MnO_4$ manganite.

(4) From a magnetic point of view the doped samples behave as spin-glass with a common freezing temperature for all of them.

(5) At room temperature the cation doping worsen the transport properties as a consequence of the chemical disorder induced in the lattice. For T < 240 K, however, the doping gives origin to an easier carrier motion in the samples due to the removal of the CO/OO and AF order present in the $La_{0.5}Sr_{1.5}MnO_4$ manganite.

Acknowledgment. Financial support from the Italian Ministry of Scientific Research (MIUR) by PRIN Projects (2004) is gratefully acknowledged. L.M. gratefully acknowledges the financial support of the "Accademia Nazionale dei Lincei". This work has been partially performed on the spallation neutron source SINQ, Paul Scherrer Institute, Villigen (CH), Switzerland. This research project has been supported by the European Commission under the sixth Framework Program through the Key Action: Strengthening the European Research Area, Research Infrastructures. Contract No. RII3-CT-2003-505925. ILL and PSI neutron facilities are acknowledged.

References and Notes

(1) Moritomo, Y.; Tomioka, Y.; Asamitsu, A.; Tokura, Y. *Phys. Rev. B* **1995**, *51*, 3297.

(2) Sternlieb, B. J.; Hill, J. P.; Wildgruber, U. C.; Luke, G. M.; Nachumi, B.; Moritomo, Y.; Tokura, Y. *Phys. Rev. Lett.* **1996**, *76*, 2169.

(3) Wilkins, S. B.; Beale, T. A. W.; Hatton, P. D.; Purton, J. A.; Bencock, P.; Prabhakaran, D.; Boothroyd, A. T. *New J. Phys.* **2005**, *7*, 80.

(4) Mahadaevan, P.; Terakura, K.; Sarma, D. D. *Phys. Rev. Lett.* **2001**, *87*, 66404.

(5) Mermin, N. D.; Wagner, H. *Phys. Rev. Lett.* **1966**, *17*, 1133.

(6) Ganguly, R.; Martin, C.; Maignan, A.; Hervieu, M.; Raveau, B. *Solid State Commun.* **2001**, *120*, 363.

(7) Malavasi, L.; Mozzati, M. C.; Polizzi, S.; Azzoni, C. B.; Flor, G. *Chem. Mater.* **2003**, *15*, 5036.

(8) Fischer, P.; Frey, G.; Koch, M.; Koennecke, M.; Pomjakushin, V.; Schefer, J.; Thut, R.; Schlumpf, N.; Buerge, R.; Greuter, U.; Bondt, S.; Berruyer, E. *Physica B* **2000**, *276*−*278*, 146.

(9) Rodriguez-Carvajal, J. *Physica B* **1993**, *192*, 55.

(10) Shannon, R. D.; Previtt, C. T. *Acta Crystallogr., Sect. B: Struct. Crystallogr. Cryst. Chem.* **1970**, *26*, 1046.

(11) Hong, C. S.; Kim, W. S.; Hur, N. H.; Choi, Y. N. *Phys. Rev. B* **2003**, *68*, 064425.

(12) Hebert, S.; Martin, C.; Maignan, A.; Retoux, R.; Hervieu, M.; Nguyen, N.; Raveau, B. *Phys. Rev. B* **2002**, *65*, 104420.

(13) Mohan Ram, R. A.; Ganguly, P.; Rao, C. N. R. *J. Solid State Chem.* **1987**, *70*, 82.

(14) Bao, W.; Chen, C. H.; Carter, S. A.; Cheong, S-W. *Solid State Commun.* **1996**, *98*, 55.

(15) Malavasi, L.; Mozzati, M. C.; Ghigna, P.; Azzoni, C. B.; Flor, G. *J. Phys. Chem. B* **2003**, *107*, 2500.

(16) Malavasi, L.; Ritter, C.; Mozzati, M. C.; Tealdi, C.; Islam, M. S.; Azzoni, C. B.; Flor, G. *J. Solid State Chem.* **2005**, *178*, 2042.

(17) Oseroff, S. B.; Torikachvili, M.; Singley, J.; Ali, S.; Cheong, S.-W.; Schultz, S. *Phys. Rev. B* **1996**, *53*, 6521.

(18) Autret, C.; Gervais, M.; Gervais, F.; Raimboux, N.; Simon, P. *Solid State Sci.* **2004**, *6*, 815.

(19) Larochelle, S.; Mehta, A.; Lu, L.; Mang, P. K.; Vajk, O. P.; Kaneko, N.; Lynn, J. W.; Zhou, L.; Greven, M. *Phys. Rev. B* **2005**, *71*, 024435.